Earth and Planetary Science Letters 295 (2010) 49–57

Contents lists available at ScienceDirect

Earth and Planetary Science Letters

journal homepage: www.elsevier.com/locate/epsl

Multi-proxy reconstruction of surface water pCO_2 in the northern Arabian Sea since 29 ka

M.R. Palmer [a,*], G.J. Brummer [b], M.J. Cooper [a], H. Elderfield [c], M.J. Greaves [c], G.J. Reichart [d], S. Schouten [b], J.M. Yu [e]

[a] NOC, School of Ocean & Earth Science, University of Southampton, European Way, Southampton, SO14 3ZH, UK
[b] Royal Netherlands Institute of Sea Research NIOZ, Departments of Geology & Marine Organic Biogeochemistry, Den Burg, Texel NL-1790 AB, The Netherlands
[c] Department of Earth Sciences, University of Cambridge, Cambridge, CB3 3EQ, UK
[d] University of Utrecht, Faculty of Earth Sciences, Department of Geochemistry, Utrecht, NL-3508 TA, The Netherlands
[e] Columbia University, Lamont Doherty Earth Observatory, Palisades, NY 10964, USA

ARTICLE INFO

Article history:
Received 25 November 2009
Received in revised form 8 March 2010
Accepted 16 March 2010
Available online 21 April 2010

Editor: P. DeMenocal

Keywords:
Arabian Sea
monsoon
carbon dioxide
palaeoceanography

ABSTRACT

We report here the results of a multi-proxy study to reconstruct surface water pCO_2 concentrations in the northern Arabian Sea. Our results show that $\delta^{11}B$ and Mg/Ca measurements of the planktonic foraminifer *Globigerinoides sacculifer* yield consistent pCO_2 values with those reconstructed from the $\delta^{13}C$ of alkenones when used in conjunction with foraminifera $\delta^{13}C$ and Cd/Ca values. They reveal that this area of the oceans has been a constant source of CO_2 to the atmosphere during the interval 5–29 ka, and that the intensity of this source was greatest between 11 and 17 ka, when atmospheric CO_2 levels were rising rapidly. We interpret our data as reflecting variation in the strength of the Asian Summer Monsoon (ASM), thus indicating that the strength of the ASM varied in phase with summer insolation over the Tibetan plateau between 5 and 29 ka. In contrast to a previous study (Clemens and Prell, 2003), we observe no significant lag between the rise in insolation and the response of the ASM. Rather, our data support a recent study by Rohling et al. (2009) that northern hemisphere climatic forcing factors play a greater role in controlling the intensity of the ASM during times of intense monsoon activity, and that the southern hemisphere forcing is more important during times of weak monsoons.

1. Introduction

It is well known that atmospheric pCO_2 has varied over glacial–interglacial time scales (Indermühle et al., 1999; Smith et al., 1999), and there is general consensus that the oceans have played a major role in regulating these changes (e.g. Broecker, 1982). While there is considerable debate concerning the exact mechanisms by which the oceans act to change atmospheric pCO_2 (e.g. Archer and Maier-Reimer, 1994; Anderson et al., 2002), there must have been changes in the surface areas of the ocean that are supersaturated or undersaturated with CO_2 with respect to the atmosphere, or changes in the magnitude of the degree of supersaturation or undersaturation.

Thanks to many years of intensive oceanographic campaigns, we now have a good understanding of the present-day geographic distribution of the pCO_2 of ocean surface waters and the CO_2 fluxes between the ocean and atmosphere (Takahashi et al., 2002). Briefly, the Arabian Sea upwelling system is second only to the Eastern Equatorial Pacific as an oceanographic source of atmospheric CO_2, with the major oceanographic sinks occurring at latitudes of 35–55°S and in the northern North Atlantic and the Norwegian Sea (Takahashi et al., 2002). Clearly, if we were able to reconstruct maps of past variations in surface ocean pCO_2 we would be in a much better position to understand the causes of glacial–interglacial changes in atmospheric pCO_2. With this in mind, several proxies have been proposed for surface water pCO_2 and applied to various areas and time scales. The two proxies that have received the most attention are the boron isotope ($\delta^{11}B$) composition of planktonic foraminifera (Palmer and Pearson, 2003) and the carbon isotope ($\delta^{13}C_{alk}$) composition of alkenones (Pagani, 2002). Recently, it has been proposed that the B/Ca ratio of planktonic foraminifera might also serve as a pCO_2 proxy (Yu et al., 2007; Foster, 2008). While these studies yield results that appear to be consistent with other oceanographic and climatologic observations, there has yet to be a study in which the efficacy of these proxies is compared at single site over the same time interval.

Here, we report the results of a multi-proxy study ($\delta^{11}B$, B/Ca and $\delta^{13}C_{alk}$) of surface water pCO_2 values in the northern Arabian Sea over the past 29 kyr. The basic aspects of the monsoon system in the Arabian Sea are well understood (Wyrtki, 1973). Strong monsoonal winds in the area lead to large seasonal changes in hydrography and particle fluxes. At the most fundamental level the monsoon is

* Corresponding author. Tel.: +44 2380596607; fax: +44 2380593059.
E-mail address: pmrp@noc.soton.ac.uk (M.R. Palmer).

0012-821X/$ – see front matter © 2010 Elsevier B.V. All rights reserved.
doi:10.1016/j.epsl.2010.03.023

controlled by changes in atmospheric pressure over the Tibetan plateau. During the northern winter increases in snow cover and cooling of the Tibetan plateau and Siberia leads to high atmospheric pressures over Central Asia. This, in turn, leads to a pressure gradient between Central Asia and the Inter Tropical Convergence Zone and drives the northeast winds of the winter monsoon. During the northern summer, the lower albedo over the Tibetan plateau causes the overlying air to heat up and rise. The resultant pressure gradient between Central Asia and the winter high over the southern ocean generates the Asian Summer Monsoon (ASM) that draws in winds towards the Tibetan plateau, leading to strong upwelling off the coast of Oman and advection of these waters into the Arabian Sea. Alongside this overall controlling mechanism, the strength of the ASM is also linked to both large scale oceanographic (e.g. ENSO) and atmospheric (e.g. southern hemisphere tropospheric flow) forcing functions that can lead to significant deviations from a simple insolation-driven monsoon model (Rodwell, 1997; Schott and McCreary, 2001).

Biological production in the Arabian Sea is generally low during winter, but the nutrient- and CO_2-rich upwelling water results in maxima in biological productivity and surface water pCO_2 values in the northern Arabian Sea between July and September (Schulte and Müller, 2001; Sarma, 2003). This regular seasonal pattern is modulated by both short- (inter-annual) and long-term (orbital-scale) variations in the strength of the ASM (Wang et al., 2005). In addition, there is considerable spatial heterogeneity in productivity and particle fluxes, as a result of limited duration eddies and wind curl events (Honjo et al., 1999). Hence, any attempt to reconstruct past variations in surface seawater conditions of the Arabian Sea from proxies must acknowledge that our understanding of the present-day spatial and temporal variations of these proxies is incomplete (Wang et al., 2005).

Nevertheless, paleoceanographic studies generally show that over the past ~250 kyr the strength of the ASM is dominated by precession cycles ~21–23 kyr, that reflect orbitally-driven variations in the strength of summer insolation over the Tibetan plateau (Reichart et al., 1997; Clemens and Prell, 2003; Yuan et al., 2004; Huybers, 2006). However, there is disagreement as to whether peaks in ASM intensity are directly in phase with maxima in summer insolation (Yuan et al., 2004) or whether the ASM maxima lag insolation curves by up to 8 kyr (Clemens and Prell, 2003).

This study seeks to apply a multi-proxy approach (δ^{11}B, B/Ca, Mg/Ca, Cd/Ca) to addressing the coherence between the intensity of the ASM and the strength of summer insolation over the interval 5–29 ka.

2. Material and methods

We have chosen a site in the northern Arabian Sea as this area is presently an important source of CO_2 from the oceans to the atmosphere (Takahashi et al., 2002). Our samples were taken from core NIOP464 collected from the southern flank of the Murray Ridge (22.15°N, 63.35°E; water depth 1470 m). Sediments from this core have been subject to detailed study, including bulk geochemical composition, foraminifer abundances, foraminifer stable isotopes, carbon-14 dating and organic geochemistry (Reichart et al., 1997; Schouten et al., 2000). Foraminifer data were determined at Southampton (δ^{11}B) and Cambridge (B/Ca, Mg/Ca and Cd/Ca), and alkenone data were determined at NIOZ using methods described by Palmer et al. (1998), Palmer and Pearson (2003) for δ^{11}B, Yu et al. (2005) for element/Ca ratios, and Schouten et al. (2000) for alkenones.

3. Results

The foraminifer and alkenone data are reported in Table 1.

Table 1

Sample	Age (ka)	*G. sacculifer*				*G. ruber*	Alkenone	
		δ^{11}B	B/Ca (μmol/mol)	Mg/Ca (mmol/mol)	Cd/Ca (μmol/mol)	δ^{13}C	$\delta^{13}C_{37}$	$U^{k'}_{37}$
X3	7.8	24.5		3.69		0.646	−22.55	0.972
X10	8.6					0.484	−22.87	0.926
X11	8.7					0.629	−24.05	0.931
X14	9.1	24.5	114.6	4.08	0.0184	0.661	−22.25	0.959
X18	9.5	24.9	104.0	3.71	0.0464	0.660	−22.28	0.986
X27	10.5	24.3	106.1	4.16		0.764	−23.44	0.949
X32	11.1	24.2	100.7	3.87	0.0441	0.697	−23.03	0.979
X40	12.0	24.5	100.8	3.92	0.0411	0.846	−24.17	0.955
X45	12.5	23.5	114.4	3.84	0.0460	0.842	−21.88	0.924
5b	13.5	23.6	105.1	3.89	0.0553	0.721	−22.96	0.969
9	14.0					0.804	−23.31	0.886
14b	14.5	25.2	96.0	4.19	0.0303	0.818	−22.86	0.928
23b	15.6	25.2	102.3	4.16	0.0424	0.898	−23.67	0.952
27b	16.0	25.3	109.9	4.04	0.0244	0.691	−23.49	0.966
30b	16.4	24.7				0.431	−23.72	0.904
36	17.0	24.9	118.5	4.05	0.0261	0.465	−24.04	0.892
40b	17.5	25.1				0.647	−23.74	0.949
51	18.7					0.430	−23.63	0.844
75	21.5	25.1				0.781	−22.01	0.923
80	22.1	25.3	105.0	3.29	0.0232	0.635	−22.34	0.851
84	22.5	25.7	105.1	3.35	0.0176	0.454	−22.37	0.895
93	23.6	24.7	110.4	3.62		0.219	−21.75	0.902
97	24.0	25.5	112.4	3.44	0.0255	0.280	−21.79	0.915
106	25.1	25.6	117.3	3.56	0.0273	0.727	−21.32	0.859
107	25.2					0.485	−23.13	0.888
114	26.0	25.0	100.8	3.25	0.0243	0.121	−21.50	0.902
116	26.2					0.421	−22.37	0.877
119	26.6	25.5	113.8	3.66	0.0289	0.530	−22.18	0.914
122	26.9					0.310	−22.81	0.879
127	27.5	25.3	109.8	3.64	0.0205	0.169	−22.91	0.925
131	28.0	24.4	112.5	3.50	0.0224	0.458	−21.72	0.912
140	29.0	25.5	119.6	3.58	0.0194	0.453	−22.03	0.924

The age model for sediments from the NIOP464 piston core reported by Reichart et al. (1998) was established by comparison of the *Neogloboquadrina dutertrei* $\delta^{18}O$ record with SPECMAP $\delta^{18}O$ chronology (Imbrie et al., 1984; Martinson et al., 1987). In this study we also used material from the trigger weight core, with cross calibration of the two cores undertaken by four independent properties (Fig. 1).

The relative abundance of the planktonic foraminifer *Globigerina bulloides* has long been used as an indicator of monsoon upwelling conditions (Prell and Curry, 1981). In contrast, foraminifer assemblages dominated by *Globigerinoides sacculifer* and *G. ruber* have often been taken to be indicative of non-upwelling conditions (Cayre et al., 1999). The dynamic and highly variable nature of the monsoon means that there are considerable spatial and temporal variations in the response of individual foraminifer species to upwelling (Peeters and Brummer, 2002). However, sediment trap studies during 1986–87 showed that seasonal variations in the absolute abundances of *G. bulloides*, *G. sacculifer* and *G. ruber* in the Arabian Sea are similar (Curry et al., 1992). The numbers of *G. sacculifer* and *G. ruber* specimens counted in the traps are typically 2 orders of magnitude lower than those of *G. bulloides* (Curry et al., 1992), so there is considerably more variance in their distribution patterns. Nevertheless, all three species show broadly coincident maxima during periods of upwelling (Fig. 2a). Hence, while the relative abundances of *G. sacculifer* and *G. ruber* in the sedimentary record are lower during upwelling periods (Ivanova et al., 2003) (because their numbers are diluted by the faster growing *G. bulloides*) they carry proxy signals that are dominated by upwelling conditions.

Studies of living *G. bulloides* and *G. sacculifer* off the Oman coast show that their depth distributions overlap at both upwelling and non-upwelling sites, although it is interesting to note that *G. bulloides* occurs at slightly shallower depths than *G. sacculifer* in upwelling locations, whereas the opposite is true at non-upwelling sites (Peeters and Brummer, 2002).

Hence, the *G. sacculifer* proxy signals likely show an understated response to upwelling conditions relative to *G. bulloides*. While it might be desirable to study pH variations recorded by the $\delta^{11}B$ of *G. bulloides*, unlike *G. sacculifer* this species has not been calibrated against this proxy in core top or culture experiments. Overall, we believe that patterns illustrated in Fig. 2 (which were derived from a sediment trap close to the core location), together with the depth distributions of living *G. sacculifer*, suggest that the proxy signals measured in this species will be dominated by variations in the intensity of the monsoon.

The C_{37-39} alkenones are biomarkers of prymnesiophyte origin, largely derived from the coccolithophorids *Emiliania huxleyi* and *Gephyrocapsa oceanica* (Brassell, 1993). Analyses of sediment trap material collected during 1994–95 from the Arabian Sea show maxima coincident with the winter and summer monsoons, with the integrated alkenone flux derived from the summer monsoon being approximately

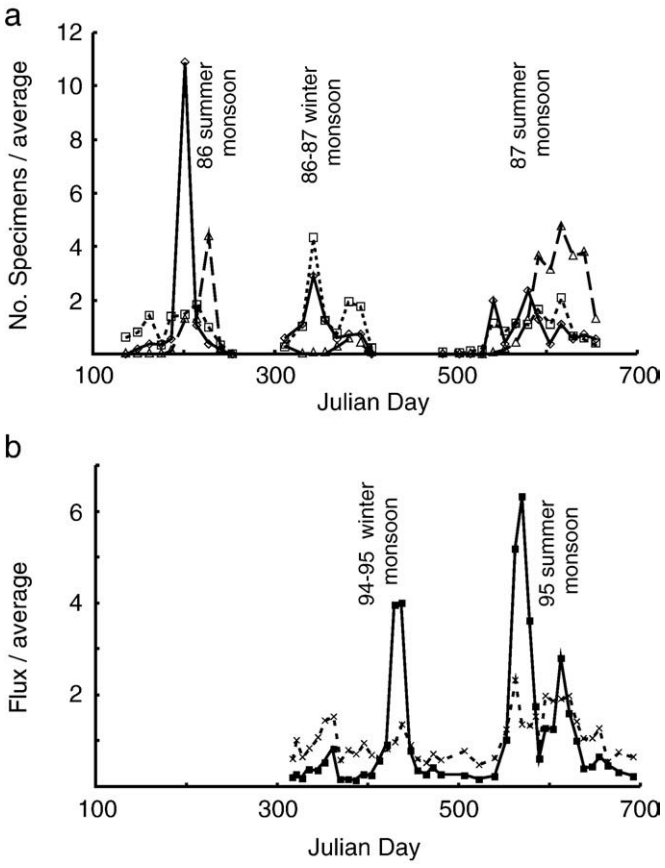

Fig. 2. a) Species fluxes of *G. bulloides* (triangles, dashed line), *G. sacculifer* (diamonds, solid line) and *G. ruber* (squares, dotted line) (>150 μm) in the western Arabian Sea (Curry et al., 1992). Note, because of the large differences in the numbers of the three species, for ease of comparison the data are plotted as the daily fluxes (for the 12–13 days of each interval) divided by the average daily flux for each species over the sampling interval. Curry et al. (1992) ascribe the absence of data in some of inter-monsoon periods to insufficient material in the sediment traps to allow for meaningful calculations. b) Flux of alkenones (solid line) and $CaCO_3$ (dashed line) in the western Arabian Sea (Prahl et al., 2000) expressed as daily fluxes (for the 12–13 days of each interval) divided by the average daily flux over the sampling interval.

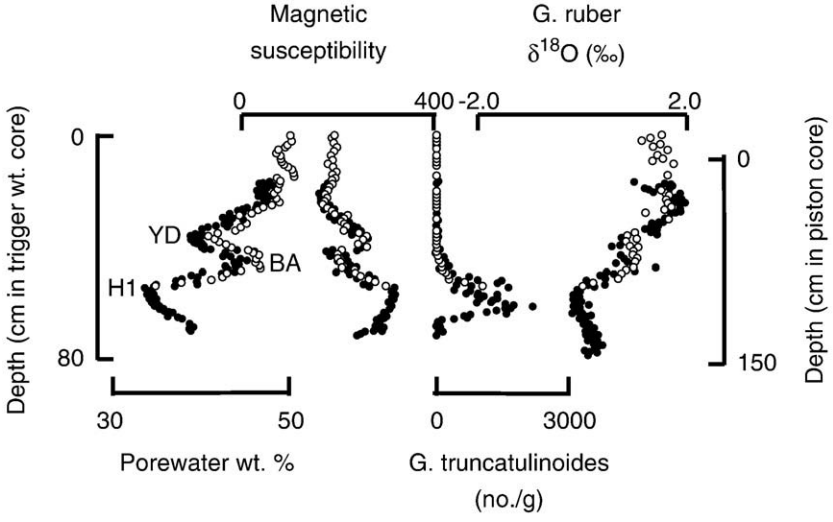

Fig. 1. Sediment properties used in cross calibrating trigger weight core (open circles) and piston core (black circles) for NIOP464.

four times greater than that from the winter monsoon (Prahl et al., 2000) (Fig. 2b). Unfortunately, there were no coincident measurements of foraminifer assemblages and alkenone fluxes from these two sediment trap studies. However, bulk $CaCO_3$ fluxes from the 1994–95 study (Prahl et al., 2000) show similar trends to the alkenone fluxes (Fig. 2b), and visual inspection of the sediment trap material suggests that foraminifers contribute significantly to the total $CaCO_3$ flux and may indeed dominate this contribution (Prahl et al., 2000).

Hence, while we concur with Wang et al. (2005) that our understanding of the spatial and temporal distribution of alkenones and the foraminifer species considered here is incomplete, the balance of the evidence suggests that the bulk of alkenones, *G. sacculifer* and *G. ruber* recovered from sediments in the northern Arabian Sea will have formed in the surface waters during summer monsoon periods.

Several studies have shown that the magnitude of the summer monsoon varies on millennial, centennial and decadal timescales in response to solar activity and other global climatic drivers, such as Heinrich events (Agnihotri et al., 2002; Herzschuh, 2006), the El Nino Southern Oscillation (Abram et al., 2007) and the Atlantic Multi-decadal Oscillation (Lu et al., 2006). As it was not always possible to measure all of the proxies in the same sub sample of core material, we have presented the proxy data as 3 point running means to smoothen these short term variations.

Sea surface temperatures (SST) were reconstructed from the alkenone $U^{k'}_{37}$-index (Brassell et al., 1986) and Mg/Ca ratios of *G. sacculifer* (Anand et al., 2003) (Fig. 3). The close agreement between these independent proxies provides further support to the coincidence of maxima in alkenone, *G. sacculifer* and *G. ruber* fluxes from the surface ocean during the ASM (Sarma, 2003; Curry et al., 1992).

The pH values derived from the $\delta^{11}B$ values (Fig. 4a) utilize the empirical pH-$\delta^{11}B$ relationship derived from culture experiments of *G. sacculifer* at different pH values that also account for the potential role of algal symbionts associated with this species (Sanyal et al., 2001). The temperature dependence of boron isotope fractionation also has to be taken into account (using the formulation of Zeebe and Wolf-Gladrow (2001) and the Mg/Ca data). In addition, a comparison study between $\delta^{11}B$ values measured at Lamont Doherty (i.e. in the Sanyal et al. (2001) study) and at Southampton revealed a consistent 2.2‰ offset between the two laboratories (Hönisch et al., 2003; Palmer and Pearson, 2003). Both this study and that of Sanyal et al. (2001) employed negative ion thermal ionization mass spectrometry (N-TIMS) to measure the boron isotope compositions of the foraminifers. This method yields $\delta^{11}B$ values that are consistently higher at equivalent pH values than those measured by multi-collector inductively coupled mass spectrometry (MC-ICP-MS) (Foster, 2008), with the latter being more consistent with the most recent experimental determination of the boron isotope fractionation factor between $B(OH)_3$ and $B(OH)_4^-$ (Klochko et al., 2006). However, several laboratories have demonstrated that the empirically calibrated N-TIMS technique does yield calculated pH values for recent foraminifer that are consistent with present-day pH values in surface seawater (Palmer and Pearson, 2003; Hönisch and Hemming, 2005). Overall, we believe that the apparent $\delta^{11}B$ offset generated by the N-TIMS method

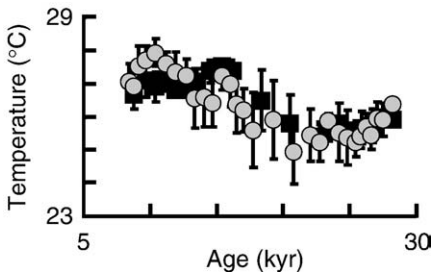

Fig. 3. Sea surface temperatures reconstructed from $U^{k'}_{37}$-index (circles) and Mg/Ca ratios of *G. sacculifer* (squares). The data are plotted as 3 point running means with 1σ error bars. The average age resolution is ±0.5 kyr.

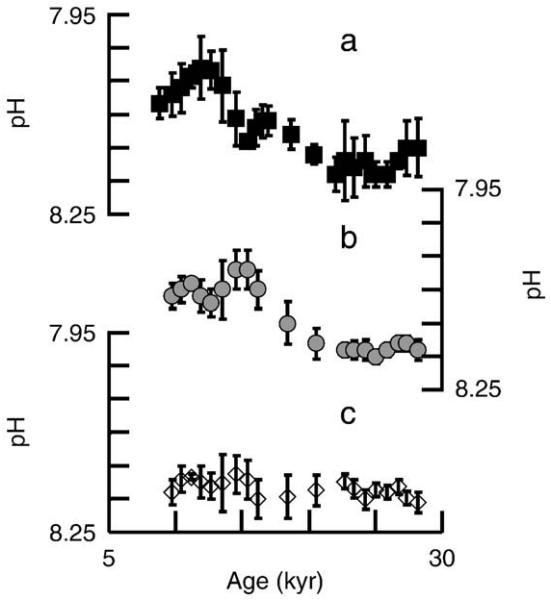

Fig. 4. a) Surface water pH reconstructed from $\delta^{11}B$ (squares). b) Surface water pH reconstructed from B/Ca (circles) using K_D-temperature relationship of Yu et al. (2007). c) Surface water pH reconstructed from B/Ca (diamonds) using K_D-temperature relationship of Foster (2008). The data are plotted as 3 pt running means with 1σ error bars. The average age resolution is ±0.5 kyr.

does not invalidate its ability to yield reliable pH records because the offset is compensated for at the calibration stage involving empirical culture experiments with the foraminifer species under consideration.

The incorporation of $B(OH)_4^-$ into foraminifer carbonate follows the equilibrium expression (Hemming and Hanson, 1992):

$$CaCO_3 + B(OH)_4^- \leftrightarrow Ca(HBO_3) + HCO_3^- + H_2O \quad (1)$$

and the surface water B/Ca ration can therefore be expressed as (Yu et al., 2007):

$$[B/Ca]_{CaCO3} = K_D \cdot [B(OH)_4^-/HCO_3^-]_{seawater} \quad (2)$$

where the distribution coefficient (K_D) is dependent on temperature and the $[B(OH)_4^-/HCO_3^-]_{seawater}$ is pH dependent. Preliminary studies on a limited data set (Yu, 2006) suggest that K_D for *G. sacculifer* follows a similar temperature relationship to *G. inflata*, which has been constrained from core top studies, and shows K_D increasing with temperature (Yu et al., 2007). However, in a down core study from the Caribbean Sea, Foster (2008) observed K_D for *G. sacculifer* decreasing with increasing temperature. More recently, Tripati et al. (2009) concluded that K_D for *G. sacculifer* was only weakly dependent on temperature. The pH values calculated from the K_D values derived from Yu et al. (2007) and Foster (2008) are illustrated in Fig. 4b and c, respectively.

Although the records are not identical, the pH values derived from the $\delta^{11}B$ data and those derived from B/Ca ratios using the Yu et al. (2007) K_D values show broadly similar trends; with pH values of ~8.2 between 29 and 22 ka, followed by a decrease to values of ~8.05–8.10 between 16 and 9 ka. In contrast, the pH values derived from the B/Ca ratios using the K_D values of Foster (2008) show essentially constant pH values of ~8.15–8.20 over the entire time span.

4. Calculation of surface water pCO_2 and cross calibration of the proxies

The seawater carbonate system has two degrees of freedom (Zeebe and Wolf-Gladrow, 2001). Hence, in addition to pH an additional parameter is required to calculate surface water pCO_2. One method is to use

alkalinity, and assume that alkalinity is proportional to salinity variations resulting from changes in the volume of the oceans as monitored by sea level variations (Waelbroeck et al., 2002; Palmer and Pearson, 2003). This approach yields a change of <20 μeq/kg in alkalinity between 30 and 5 ka (the age range considered in this study). However, it is important to note that the calculated pCO_2 is relatively insensitive to reasonable uncertainties in alkalinity. For example, an uncertainty of ±50 μeq/kg in alkalinity leads to an uncertainty of only ±5.5 ppm in pCO_2 at a pH of 8.2, using the carbonate equilibrium constants described in Zeebe and Wolf-Gladrow (2001) — which is well within the analytical error of measurements of either the $\delta^{11}B$ value or B/Ca ratio (typically ±20 ppm in both cases). Similarly, uncertainties of ±2 °C in temperature and ±1 salinity unit, lead to corresponding uncertainties of only ±3.2 and ±2.5 ppm CO_2, respectively, when considering the dependence of carbonate and borate equilibria on these parameters.

The surface water pCO_2 values calculated from the pH reconstructions from the $\delta^{11}B$ values and B/Ca ratios, and assuming alkalinity proportional to ocean volume as given by sea level variations (Waelbroeck et al., 2002) are illustrated in Fig. 5. Again, records derived from the $\delta^{11}B$ and Yu et al. (2007) K_D values are more similar to one another than the pCO_2 values derived from the Foster (2008) K_D values.

In addition to calculating pCO_2 independently from both the $\delta^{11}B$ and B/Ca proxies, they can be combined to yield pCO_2 values. The $\delta^{11}B$ values can then be used to derive pH, and hence $[B(OH)_4^-]$, and the B/Ca values substituted into Eq. (2) to yield $[HCO_3^-]$. With two degrees of freedom defined within the carbonate system it is then possible to calculate pCO_2 without assuming any value for alkalinity (Foster, 2008). The surface water pCO_2 values calculated from the combined use of the B/Ca and $\delta^{11}B$ proxies are illustrated in Fig. 6. The close agreement between the two curves derived from the different formulations of the B/Ca K_D-temperature relationship clearly illustrate the dominant role played by pH (as defined by the $\delta^{11}B$ data) in defining pCO_2 values. This observation suggests that the B/Ca proxy does not greatly aid in constraining surface water pCO_2, regardless of the nature of the K_D-temperature relationship.

Surface water pCO_2 records can also be reconstructed from the alkenone carbon isotope composition ($\delta^{13}C_{alk}$) based on the records of

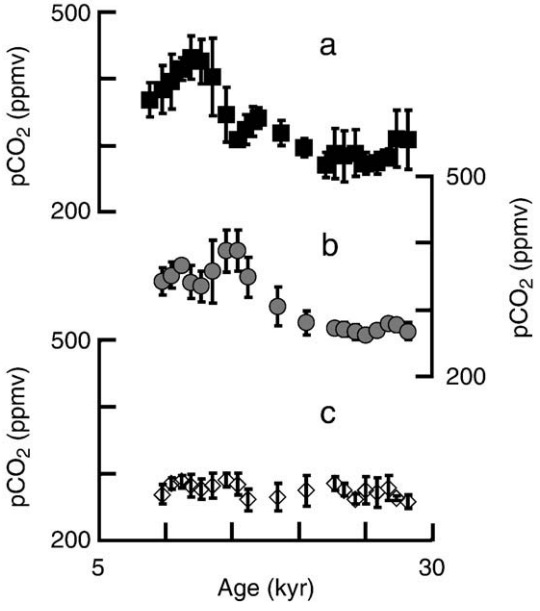

Fig. 5. a) Surface water pCO_2 values calculated from pH values derived from $\delta^{11}B$ values measured in *G. sacculifer*. b) Surface water pCO_2 values calculated from pH values derived from B/Ca values measured in *G. sacculifer* and K_D values of Yu et al. (2007). c) Surface water pCO_2 values calculated from pH values derived from B/Ca values measured in *G. sacculifer* and K_D values of Foster (2008). In all three cases alkalinity is assumed to be proportional to salinity as derived from variations in sea level. The data are plotted as 3 point running means with 1σ error bars.

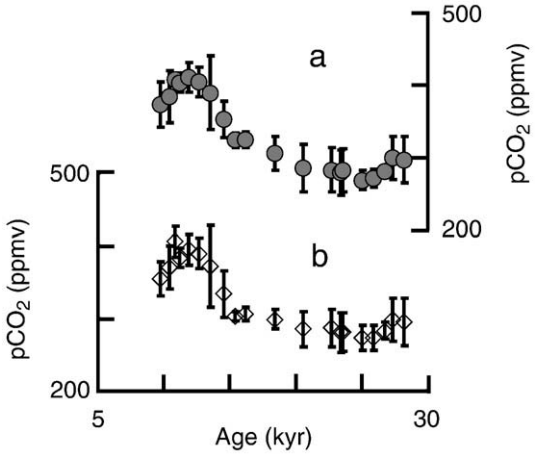

Fig. 6. Surface water pCO_2 values (3 point running means with 1σ error bars) calculated from combined use of the $\delta^{11}B$ and B/Ca proxies. a) Using the Yu et al. (2007) B/Ca K_D-temperature relationship. b) Using the Foster (2008) B/Ca K_D-temperature relationship.

carbon isotope fractionation during photosynthetic carbon fixation (Pagani, 2002). In addition to $\delta^{13}C_{alk}$, this method requires a record of the $\delta^{13}C$ of dissolved inorganic carbon ($\delta^{13}C_{DIC}$) (derived here from the $\delta^{13}C$ of *G. ruber*) and dissolved phosphate $[PO_4^{3-}]$ (derived here from the Cd/Ca ratio of *G. sacculifer* (Elderfield and Rickaby, 2000)).

The relevant equations are (Pagani, 2002):

$$\varepsilon_{p37.2} = [(\delta d + 1000 / \delta p + 1000) - 1] \times 10^3 \quad (3)$$

Where, δd is the $\delta^{13}C$ of the inorganic carbonate ($\delta^{13}C_{DIC}$) in the mixed layer (obtained from $\delta^{13}C$ *G. ruber*), and δp is the $\delta^{13}C$ of the haptophyte organic matter enriched by 4.2‰ relative to alkenone $\delta^{13}C$. Surface water pCO_2 can then be calculated from:

$$\varepsilon_{p37.2} = \varepsilon_f - b / [CO_2(aq)] \quad (4)$$

Where, ε_f is the carbon isotope fractionation due to carboxylation (25–27‰, Popp et al., 1998; Goericke et al., 1994).

$$b = \left\{\left(118.52\left[PO_4^{3-}\right]\right) + 84.07\right\} / (25 - \varepsilon_{p37.2}) \quad (5)$$

Values for pCO2 are then obtained from the appropriate carbonate ion equilibrium constants (Zeebe and Wolf-Gladrow, 2001), with salinity obtained from the sea level curve and temperature from the $U^{k'}_{37}$-index measured in the alkenones.

A 1‰ uncertainty in $\delta^{13}C_{DIC}$ would lead to an ~25 ppm uncertainty in the calculated pCO_2. This level of uncertainty is similar to the 0.5–1.5‰ offset in $\delta^{13}C$ values that are observed in foraminifer species hosting algal symbionts (such as *G. ruber*), hence variations of this magnitude have a minimal impact on estimated pCO_2 from alkenones (Pagani et al., 1999). By comparison, a typical uncertainty of ±10% in the Cd/Ca would lead to a similar level of uncertainty in the calculated $[PO_4^{3-}]$ concentration and a 15 ppm uncertainty in the calculated pCO_2 value. The surface water pCO_2 values calculated utilizing this approach is illustrated in Fig. 7.

The pCO_2 values reconstructed from the $\delta^{11}B$ record (Fig. 5a) and the alkenone record (Fig. 7) yield broadly similar results — with calculated pCO_2 values rising from ~300 ppm between 29–17 ka, to maximum values of ~400 ppm between 16–12 ka, before falling back to values of ~350 ppm in the most recent samples. These two reconstructions are entirely independent, and are not based on any shared data (other than the age model). This observation is supportive of the hypothesis that the $\delta^{11}B$ and $\delta^{13}C_{alk}$ proxies are capable of yielding reliable reconstructions of surface water pCO_2 values when

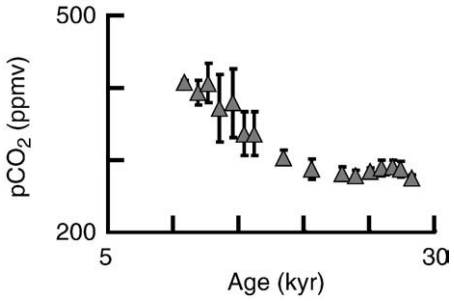

Fig. 7. Surface water pCO_2 values (3 point running means with 1σ error bars) calculated from combined use of the $\delta^{13}C_{alk}$ and $\delta^{13}C_{DIC}$ and Cd/Ca proxies.

used in appropriate combination with other proxies for temperature, $\delta^{13}C_{DIC}$ and nutrient concentrations.

As noted above, Cd/Ca ratios of *G. sacculifer* can be used to reconstruct surface water $[PO_4^{3-}]$ (Elderfield and Rickaby, 2000). Alternatively, surface water $[PO_4^{3-}]$ can be reconstructed if the surface water pCO_2 values reconstructed from the $\delta^{11}B$ proxy are assumed to be reliable, and then inverting the alkenone data to derive the $[PO_4^{3-}]$ values required to achieve the same pCO_2 values. Again, the two independent $[PO_4^{3-}]$ reconstructions show broadly consistent patterns, with relatively low concentrations in the period 29–16 ka, a peak at ~14–11 ka, and a return to lower values in the most recent samples (Fig. 8).

5. Discussion

It has been estimated that there is currently a flux of ~70×10^{12} g C yr^{-1} to the atmosphere from the Arabian Sea, of which the ASM contributes ~60% (Sarma, 2003). This flux of CO_2 is second only to the Eastern Equatorial Pacific upwelling system as an oceanic source of atmospheric CO_2 (Takahashi et al., 2002; Sarma, 2003). Fig. 9 illustrates the pooled pCO_2 surface water reconstructions from the $\delta^{11}B$ and $\delta^{13}C_{alk}$ proxies, together with the variations in ΔpCO_2 (the difference between the pCO_2 of the surface waters and contemporaneous atmosphere, as derived from the ice core record (Indermühle et al., 1999; Smith et al., 1999)). It is apparent that this area of the ocean has been a source of CO_2 to the atmosphere throughout the entire time interval covered by this study, although the magnitude of this flux has varied. It is noteworthy that the maxima in pCO_2 and ΔpCO_2 are coincident with the second pulse of the rapid post glacial increase in atmospheric CO_2 (Monnin et al., 2004), hence it is possible that increased intensity of the ASM may have contributed to this change.

In addition to ΔpCO_2, the flux of CO_2 between surface seawater and the atmosphere depends on the CO_2 gas transfer velocity, which is in turn dependent on the surface wind speed (Wanninkhof, 1992). Because surface wind speeds are greater over the Arabian Sea during periods of enhanced monsoon activity (Schott and McCreary, 2001), the magnitude of the CO_2 flux from the Arabian Sea to the atmosphere

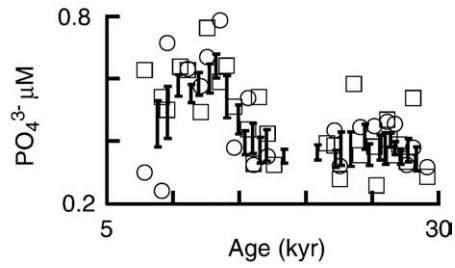

Fig. 8. Surface seawater $[PO_4^{3-}]$ concentrations reconstructed from Cd/Ca ratios of *G. sacculifer* (circles), inversion of the alkenone data (squares) (see text for details), and 3 pt running mean of both reconstructions with 1σ error bars. The average age resolution is ±0.5 kyr.

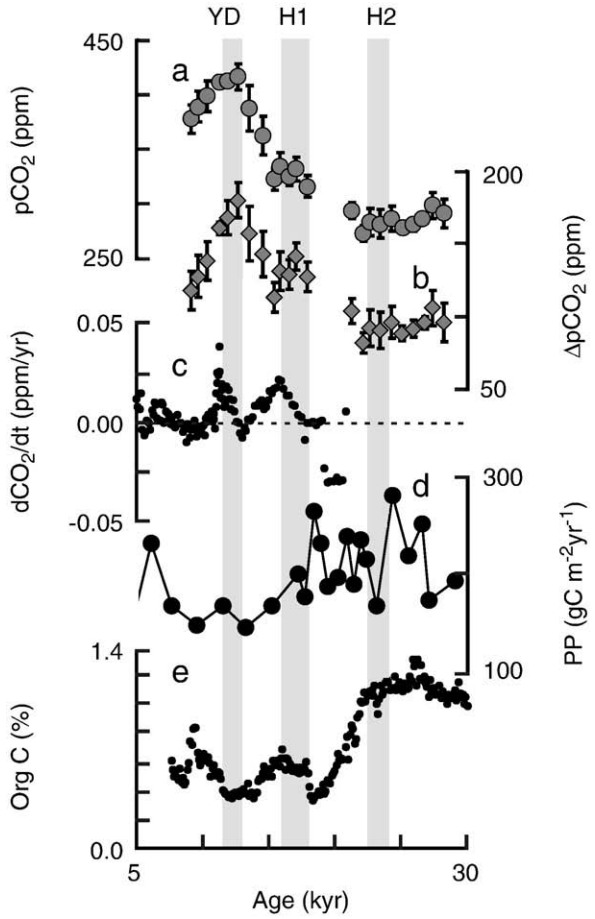

Fig. 9. a) 3 pt running mean of the pooled surface water pCO_2 values calculated from the two methods discussed in the text. b) 3 pt running mean of the ΔpCO_2 between pCO_2 of surface waters and contemporaneous atmosphere (Indermühle et al., 1999; Smith et al., 1999). c) Rate of change of atmospheric CO_2 as determined from a 7 pt running mean of high resolution data from Antarctic ice cores (Monnin et al., 2004). d) Primary productivity variations in the northern Arabian Sea as reconstructed from application of principal component analysis and transfer functions to planktic foraminifera assemblages (Ivanova et al., 2003). e) Percentage organic carbon in sediments from NIOP 464 sediment core (Reichart et al., 1997, 1998).

would likely have been greater than implied by the change in ΔpCO_2 alone. It is important to note, however, that the net flux of CO_2 to the atmosphere is also dependent on any enhanced biological carbon fixation and burial associated arising from the concomitant high nutrient concentrations of the upwelled water (for example, as illustrated by the higher surface water $[PO_4^{3-}]$ shown in Fig. 8). Indeed, the present-day Arabian Sea is an area of significant biological drawdown of surface water CO_2 (Takahashi et al., 2002). However, the amount of organic carbon preserved in NIOP464 sediments is actually lower during the period of high pCO_2 concentrations (Fig. 9e) (Reichart et al., 1997, 1998). Ivanova et al. (2003) suggest that this may be due to reduced primary productivity in the northern Arabian Sea, but Schenau et al. (2005) also noted that there was a disconnect between the burial efficiency of phosphorus and productivity in the Arabian Sea during the Late Quaternary, that was due in part to fluctuations in bottom water oxygen concentrations. Regardless of the mechanism, it is apparent that high surface water pCO_2 concentrations generated from increased intensity of the ASM did not result in a concomitant increase in burial of organic carbon. Hence, the increased surface water pCO_2 concentrations likely led a net increase in the flux of CO_2 to the atmosphere during ~11–18 ka.

The potential magnitude of the effect of enhanced ASM intensity on atmospheric CO_2 levels may be gauged by comparison with the present-day. Fossil fuel burning and cement manufacture

averaged ~6×10^{15} g C yr^{-1}, leading (among other causes) to a rise of ~0.8 ppm yr^{-1} in atmospheric CO_2 (Boden and Marland, 2009; Keeling et al., 2009). The present-day CO_2 flux to the atmosphere from the Arabian Sea due to the ASM is ~40×10^{12} g C yr^{-1}, arising from a ΔpCO_2 of ~100 ppm (Sarma, 2003). If the CO_2 flux scales directly with ΔpCO_2, the average ΔpCO_2 of 140 ppm between ~11–18 ka would correspond to an increase of ~25×10^{12} g C yr^{-1} in the CO_2 flux arising from the ASM. By analogy with the present-day rise in atmospheric CO_2 levels, this would suggest the contribution of the more intense ASM to rising atmospheric CO_2 levels between 11–18 ka was ~0.003 ppm yr^{-1}, compared to an average rise of ~0.010 ppm yr^{-1} over this interval (Monnin et al., 2004; Fig. 9c).

There has been considerable debate regarding the relative timing of the ASM and the orbitally-driven temporal variations in the strength of insolation over the Tibetan plateau (e.g., Ruddiman, 2006; Clemens and Prell, 2007). While this study only covers a relatively brief period, it does cover most of a full precession cycle and, by dint of covering the most recent cycle, it is the most accurately dated period of the marine record.

Fig. 10 is a compilation of the pCO_2 and $[PO_4^{3-}]$ records generated in this study, together with other marine and terrestrial records spanning the relevant time interval. Also included in Fig. 10 is the summer insolation record over the Tibetan plateau (Fig. 10c) (Huybers, 2006) and the Asian Summer Monsoon Stack (SMS) (Fig. 10d) generated by Clemens and Prell (2003). The SMS is a compilation of five marine proxies ($\delta^{15}N$, opal mass accumulation rate, percentage abundance of *G. bulloides*, lithogenic grain size, and excess Ba mass accumulation rate) obtained from two sediment cores from the Owen Ridge off the Oman margin (Clemens and Prell, 2003). These proxies were then combined (stacked) and subjected to a principal components analysis to yield the SMS. Over the 350,000 time period considered by Clemens and Prell (2003), the SMS lagged the precession-driven, northern hemisphere summer insolation maximum by an average of 121°, or 7.7 ka. This lag has been interpreted as being due to a complex interplay between land surface and ocean feedbacks that produce climatic responses that are of the same order as radiative forcing, such that the latent heat influx from the southern hemisphere leads to a delay in the response of the ASM to the rise in insolation (Clemens and Prell, 2003, 2007). This offset is seen clearly in Fig. 10 where, for the last precession cycle, the SMS maximum lags the insolation maximum by 3 kyr.

In contrast, the oxygen isotope compositions of stalagmites from China extending back to 224 ka, have been used to argue that there is no discernable delay between the intensity of the ASM and northern hemisphere insolation (Wang et al., 2001; Yuan et al., 2004; Wang et al., 2008). Clemens and Prell (2007) countered this observation by arguing that these Chinese speleothems monitor precipitation associated with the East Asian monsoon, that has a West Pacific moisture source, and do not therefore provide a valid record of the strength of the ASM. However, recent $\delta^{18}O$ data from a stalagmite from Socotra Island, Yemen, which is far removed from the influence of the East Asian monsoon, show close agreement with the Chinese stalagmite data and have been interpreted to suggest that both localities record the isotope record of precipitation, which is in turn driven by the strength of the ASM (Shakun et al., 2007). Although the Socotra record is not complete over the time period considered in this study, Fig. 10e clearly shows the $\delta^{18}O$ values decreasing in phase with the rise in insolation (Huybers, 2006) and with the pCO_2 and $[PO_4^{3-}]$ proxy records from this study, but well before the rise in the SMS (Clemens and Prell, 2003).

The Socotra speleothem record also accords with $\delta^{15}N$ data from core NIOP905 from the Somalia margin that shows the strength of the ASM declining after ~ 10 ka (Ivanochko et al., 2005) (Fig. 10f), before the SMS reaches its maximum value. Shakun et al. (2007) noted that both these records contain a strong signal of the Younger Dryas, and suggested that, in addition to changes in insolation, the strength of the ASM was strongly influenced by the extent of northern hemisphere climatic forcing during the last deglaciation.

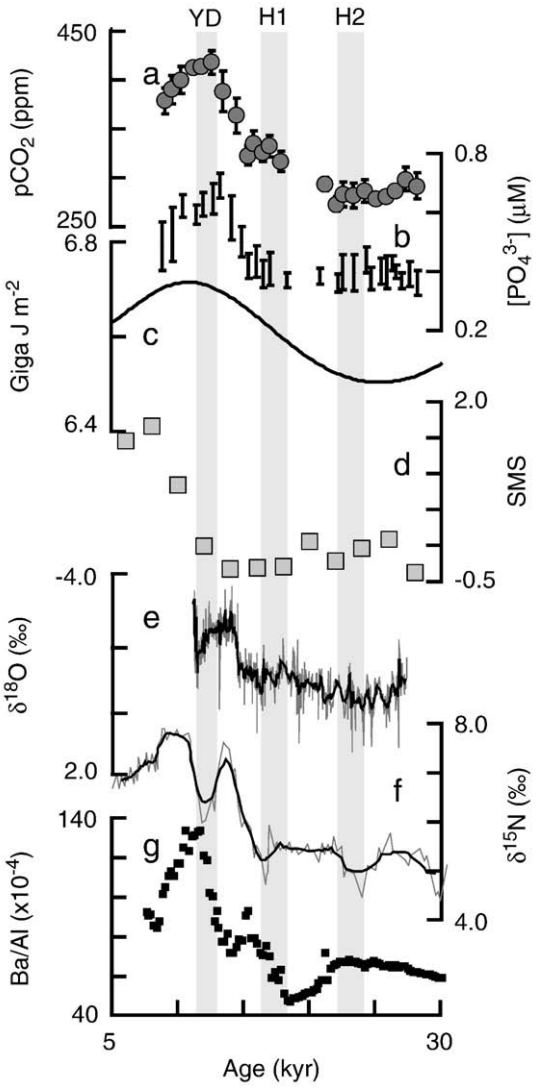

Fig. 10. a) 3 point running mean (1σ error bars) of pCO_2 values of surface seawater. b) 3 point running mean (1σ error bars) of $[PO_4^{3-}]$ levels of surface seawater. c) Summer insolation variations at 30°N (Huybers, 2006). d) Arabian Sea summer monsoon stack (SMS) (Clemens and Prell, 2003). e) Socotra stalagmite $\delta^{18}O$ record (Shakun et al., 2007). f) δ^{15} N record from NIOP905 sediment core (Ivanochko et al., 2005). g) Ba/Al ratios of sediments from NIOP464 sediment core. The composite pCO_2 and PO_4 records obscure the Younger Dryas and Heinrich events seen in the Somalia margin proxies, but as none of these high resolution events are seen in the individual proxy records measured at NIOP464, except for the physical properties (Fig. 1), this suggests that the lower sedimentation rate open ocean site at NIOP464 tends to average out conditions seen in the higher sedimentation rate margin sites.

As noted above, one of the proxies used by Clemens and Prell (2003) to compile the SMS is the excess Ba concentration measured in sediments. In this study, we have extended the Ba/Al record of Reichart et al. (1997) from NIOP464 piston core to 7.6 ka by using sediments from the trigger weight of the piston core, and replotting the data according to the age model of Reichart et al. (1998) (Fig. 10g). Again, the age of the maximum in this proxy coincides with timing of the maximum insolation over the Tibetan plateau during the last deglaciation (Huybers, 2006) and occurs significantly ahead of the peak in the SMS signal (Clemens and Prell, 2003).

There are several possible reasons for the apparent discrepancy between the proxy records from this study and others (Wang et al., 2001; Ivanochko et al., 2005; Yuan et al., 2004; Shakun et al., 2007; Wang et al., 2008) that appear to show the AMS in phase with insolation, and the hypothesis that a significant lag exists between the peak in insolation and the strength of the ASM (Clemens and Prell, 2003). It is

possible that past variations in the surface water pCO_2 and $[PO_4^{3-}]$ concentrations and Ba/Al ratios at the site of NIOP464 do not directly reflect the intensity of the ASM if, for example, there were temporal variations in the depth from which the upwelled waters were derived and the advection pathway of the upwelled waters into the Arabian Sea. Indeed, variations in both these parameters are seen on an inter-annual basis in the modern Arabian Sea (Schott and McCreary, 2001). However, if this were the case then it would also call into question the marine records used to generate the SMS index (Clemens and Prell, 2003), and indeed many other marine records of monsoon activity.

The time period covered in this study is too short to resolve the long-standing debate regarding the phasing of the ASM with insolation and/or other climate forcing functions over multiple orbital cycles. Nevertheless, the observations presented here are consistent with a recent study which suggests that northern hemisphere climatic controls exhibit a stronger control over ASM intensity when the monsoon is strong, thus explaining the apparent synchronicity between the NIOP 464 ASM proxies and northern hemisphere insolation (Fig. 10), but that southern hemisphere processes exhibit a greater control over ASM intensity when the monsoon is weak (Rohling et al., 2009).

6. Conclusions

We have demonstrated that the $\delta^{11}B$ and $\delta^{13}C_{alk}$ proxies can yield reliable and self consistent reconstructions of surface water pCO_2 when used in combination with other paleoceanographic proxies of temperature (Mg/Ca and $U^{k'}_{37}$-index), $\delta^{13}C_{DIC}$ (from foraminifera $\delta^{13}C$) and nutrient concentrations (from foraminifera Cd/Ca).

These proxies have been applied to sediments separated from the NIOP464 core taken from the northern Arabian Sea, and show that this area has been a constant source of CO_2 to the atmosphere over the interval 5–29 ka. The magnitude of this source shows considerable variation with time, and was greatest between ~11–17 ka. This period coincides with the time when atmospheric CO_2 levels were rapidly increasing during the last deglaciation.

The reconstructed surface water pCO_2 and $[PO_4^{3-}]$ concentrations show maximum values that are coincident with the maximum in northern hemisphere summer insolation over the Tibetan plateau. The timing of these maxima is consistent with other proxy data from the region from both marine sediment cores and speleothems. In contrast, the data presented here do not support the 3 kyr lag between the timing of the summer monsoon maximum and northern hemisphere summer insolation proposed by Clemens and Prell (2003).

Our observations are consistent with the hypothesis that northern hemisphere climatic forcing functions play a greater role in controlling of the Asian Summer Monsoon during times of strong monsoons, and that the southern hemisphere factors are more important during times of weak monsoons (Rohling et al., 2009).

Acknowledgements

This study was funded by the 6C program of the EC, and we thank J. Bijma for his role in coordinating this project. JA Milton and J Ossebaar assisted with the analyses. Thanks also to EJ Rohling, GL Foster and H Palike for helpful discussions and feedback. This manuscript was also greatly improved as the result of three constructive anonymous reviews.

References

Abram, N.J., Gagan, M.K., Liu, Z., Hantro, W.S., McCulloch, M.T., Suwargadi, B.W., 2007. Seasonal characteristics of the Indian Ocean Dipole during the Holocene epoch. Nature 445, 299–302.

Agnihotri, R., Dutta, K., Bhushan, R., Somayajulu, B.L.K., 2002. Evidence for solar forcing on the Indian monsoon during the last millenium. Earth Planet. Sci. Lett. 198, 521–527.

Anand, P., Elderfield, H., Conte, M.H., 2003. Calibration of Mg/Ca thermometry in planktonic foraminifera from a sediment trap time series. Paleoceanography 18, 1050. doi:10.1029/2002PA000846.

Anderson, R.F., Chase, Z., Fleisher, M.Q., Sachs, J., 2002. The Southern Ocean's biological pump during the Last Glacial Maximum. Deep-Sea Res. II 49, 1909–1938.

Archer, D., Maier-Reimer, E., 1994. Effect of deep-sea sedimentary calcite preservation on atmospheric CO_2 concentration. Nature 367, 260–263.

Boden, T., Marland, G., 2009. Global CO_2 emissions from fossil-fuel burning, cement manufacture and gas flaring: 1751-2006. doi:10.3334/CDIAC/00001.

Brassell, S.C., 1993. Applications of biomarkers for delineating marine paleoclimatic fluctuations during the Pleistocene. In: Engel, M.H., Macko, S.A. (Eds.), Organic Geochemistry. Plenum Press, New York, pp. 699–738.

Brassell, S.C., Eglinton, G., Marlowe, I.T., Pflaumann, U., Sarntheim, M., 1986. Molecular stratigraphy—a new tool for climatic assessment. Nature 320, 129–133.

Broecker, W.S., 1982. Glacial to interglacial changes in ocean chemistry. Prog. Oceangr. 2, 151–197.

Cayre, O., Beaufort, L., Vincent, E., 1999. Paleoproductivity in the Equatorial Indian Ocean for the last 260,000 yr: a transfer function based on planktonic foraminifera. Quat. Sci. Rev. 18, 839–857.

Clemens, S.C., Prell, W.L., 2003. A 350, 000 year summer-monsoon multi-proxy stack from the Owen Ridge, Northern Arabian Sea. Mar. Geol. 201, 35–51.

Clemens, S.C., Prell, W.L., 2007. The timing of orbital-scale Indian monsoon changes. Quat. Sci. Rev. 26, 275–278.

Curry, W.B., Ostermann, D.R., Guptha, M.V.S., Ittekkot, V., 1992. Foraminferal production and monsoonal upwelling in the Arabian Sea: evidence from sediment traps (suppl. data). Geol. Soc. Lond. Spec. Publ. 64, 93–106.

Elderfield, H., Rickaby, R.E.M., 2000. Oceanic Cd/P ratio and nutrient utilization in the glacial Southern Ocean. Nature 405, 305–310.

Foster, G.L., 2008. Seawater pH, pCO_2 and $[CO_3^{2-}]$ variation in the Caribbean Sea over the last 130 kyr: a boron isotope and B/Ca study of planktic foraminifera. Earth Planet. Sci. Lett. 271, 254–266.

Goericke, R., Montoya, J.P., Fry, B., 1994. Physiology of isotope fractionation in algae and cyanobacteria. In: Lajtha, K., Michener, B. (Eds.), Stable Isotopes in Ecology. Blackwell, Malden, Mass, pp. 187–221.

Hemming, N.G., Hanson, G.N., 1992. Boron isotopic composition and concentration in modern marine carbonates. Geochim. Cosmochim. Acta 56, 537–543.

Herzschuh, U., 2006. Palaeo-moisture evolution in monsoonal Central Asia during the last 50,000 years. Quat. Sci. Rev. 25, 163–178.

Hönisch, B., Hemming, N.G., 2005. Surface ocean pH response to variations in pCO_2 through two full glacial cycles. Earth Planet. Sci. Lett. 236, 305–314.

Hönisch, B., Bijma, J., Russell, A.D., Spero, H.J., Palmer, M.R., Zeebe, R.E., Eisenhauer, A., 2003. The influence of symbiont photosynthesis on the boron isotopic composition of foraminifera shells. Mar. Micropaleontol. 49, 87–96.

Honjo, S., Dymond, J., Prell, W., Ittekkot, V., 1999. Monsoon-controlled export fluxes to the interior of the Arabian Sea. Deep-Sea Res. II 46, 1859–1902.

Huybers, P., 2006. Early Pleistocene glacial cycles and the integrated summer insolation forcing. Science 313, 508–511.

Imbrie, J., Hays, J.D., Martinson, D.G., McIntyre, A., Mix, A.C., Morley, J.J., Pisias, N.G., Prell, W.L., Shackleton, N.J., 1984. The orbital theory of Pleistocene climate: support from a revised chronology of the marine $\delta^{18}O$ record. In: Berger, A.L., Imbrie, J., Hays, J., Kukla, G., Saltzman, B. (Eds.), Milankovitch and Climate, Part I. Reidel, Dordrecht, pp. 269–305.

Indermühle, A., Stocker, T.F., Joos, F., Fischer, H., Smith, H.J., Wahlen, M., Deck, B., Mastroianni, D., Tschumi, J., Blunier, T., Meyer, R., Stauffer, B., 1999. Holocene carbon-cycle dynamics based on CO_2 trapped in ice at Taylor Dome, Antarctica. Nature 398, 121–126.

Ivanochko, T.S., Ganeshram, R.S., Brummer, G.J.A., Ganssen, G., Jung, S.J.A., Moreton, S.G., Kroon, D., 2005. Variations in tropical convection as an amplifier of global climate change at the millennial scale. Earth Planet. Sci. Lett. 235, 302–314.

Ivanova, E., Schiebel, R., Singh, A.D., Schmiedl, G., Niebler, H.S., Hemleben, C., 2003. Primary production in the Arabian Sea during the last 135,000 years. Palaeogeogr. palaeoclimatol. palaeoecol. 197, 61–82.

Keeling, R.F., Piper, S.C., Bollenbacher, A.F., Walker, J.S., 2009. Atmospheric CO_2 records from sites in the SIO air sampling network. Trends: A Compendium of Data on Global Change. CDIAC, ORNL, US Dept. Energy, Oak Ridge, TN, USA. (cdiac.ornl.gov/trends/co2/sio-mlo.html).

Klochko, K., Kaufman, A.J., Yoa, W., Byrne, R.H., Tossell, J.A., 2006. Experimental measurement of boron isotope fractionation in seawater. Earth Planet. Sci. Lett. 248, 261–270.

Lu, R., Dong, B., Ding, H., 2006. Impact of the Atlantic Multidecadal Oscillation on the Asian summer. Geophys. Res. Lett. 33, L24701.

Martinson, D.G., Pisias, N.G., Hays, J.D., Imbrie, J., Moore, T.C., Shackleton, N.J., 1987. Age dating and the orbital theory of the ice ages: development of a high-resolution 0–300,000 year chronostratigraphy. Quat. Res. 27, 1–29.

Monnin, E., Steig, E.J., Siegenthaler, U., Kawamura, K., Schwander, J., Stauffer, B., Stocker, T.F., Morse, D.L., Barnola, J.M., Bellier, B., Raynaud, D., Fischer, H., 2004. Evidence for substantial accumulation rate variability in Antarctica during the Holocene through synchronization of CO_2 in the Taylor Dome, Dome C and DML ice cores. Earth Planet. Sci. Lett. 224, 45–54.

Pagani, M., 2002. The alkenone–CO_2 proxy and ancient atmospheric carbon dioxide. Trans. Roy. Soc. Lond. Ser. A 360, 575–602.

Pagani, M., Arthur, M.A., Freeman, K.H., 1999. Miocene evolution of atmospheric carbon dioxide. Paleoceanography 14, 272–292.

Palmer, M.R., Pearson, P.N., 2003. A 23, 000-year record of surface ocean water pH and pCO2 in the Western Equatorial Pacific Ocean. Science 300, 480–482.

Palmer, M.R., Pearson, P.N., Cobb, S.J., 1998. Reconstructing past ocean pH-depth profiles. Science 282, 1468–1471.

Peeters, F.J.C., Brummer, G.J.A., 2002. The seasonal and vertical distribution of living planktic foraminifera in the NW Arabian Sea. Geol. Soc. Lond. Spec. Publ. 195, 463–497.

Popp, B.N., Laws, E.A., Bidigare, R.R., Dore, J.E., Hanson, K.L., Wakeham, S.G., 1998. Effect of phytoplankton cell geometry on carbon isotopic fractionation. Geochim. Cosmochim. Acta 62, 69–77.

Prahl, F.G., Dymond, J., Sparrow, M.A., 2000. Annual biomarker record for export production in the Central Arabian Sea. Deep-Sea Res. II 47, 1581–1604.
Prell, W.L., Curry, W.B., 1981. Faunal and isotopic indices of monsoonal upwelling: western Arabian Sea. Oceanol. Acta 4, 91–98.
Reichart, G.J., den Dulk, M., Visser, H.J., van der Weijden, C.H., Zachariasse, W.J., 1997. A 225 kyr record of dust supply, paleoproductivity and the oxygen minimum zone from the Murray Ridge (northern Arabian Sea). Palaeogeogr. palaeoclimatol. palaeoecol. 134, 149–169.
Reichart, G.J., Lourens, J., Zachariasse, W.J., 1998. Temporal variability in the northern Arabian Sea Oxygen Minimum Zone (OMZ) during the last 225,000 years. Paleoceanography 13, 607–621.
Rodwell, M.J., 1997. Breaks in the Asian monsoon: the influence of Southern Hemisphere weather systems. J. Atmos. Sci. 54, 2597–2611.
Rohling, E.J., Liu, Q.S., Roberts, A.P., Stanford, J.D., 2009. Controls on the East Asian monsoon during the last glacial cycle, based on comparison between Hulu Cave and polar ice-core records. Quat. Sci. Rev. 28, 3291–3302.
Ruddiman, W.F., 2006. What is the timing of orbital-scale monsoon changes? Quat. Sci. Rev. 25, 657–658.
Sanyal, A., Bijma, J., Spero, H., Lea, D.W., 2001. Empirical relationship between pH and the boron isotopic composition of *Globigerinoides sacculifer*: Implications for the boron isotope paleo-proxy. Paleoceanography 16, 515–519.
Sarma, V.V.S.S., 2003. Monthly variability in surface pCO_2 and net air-sea CO_2 flux in the Arabian Sea. J. Geophys. Res. 108, 3255. doi:10.1029/2001JC001062.
Schenau, S.J., Reichart, G.J., de Lange, G.J., 2005. Phosphorus burial as a function of paleoproductivity and redox conditions in Arabian Sea sediments. Geochim. Cosmochim. Acta 69, 919–931.
Schott, F.A., McCreary, J.P., 2001. The monsoon circulation of the Indian Ocean. Progr. Oceanogr. 51, 1–123.
Schouten, S., Hoefs, M.J.L., Damsté, J.S.S., 2000. A molecular and stable carbon isotope study of lipids in late Quaternary sediments from the Arabian Sea. Organic Geochem. 31, 509–521.
Schulte, S., Müller, P.J., 2001. Variations of sea surface temperature and primary productivity during Heinrich and Dansgaard–Oeschger events in the northern Arabian Sea. Geo-Mar. Lett. 21, 168–175.
Shakun, J.D., Burns, S.J., Fleitmann, D., Kramers, J., Matter, A., Al-Subary, A., 2007. A high-resolution, absolute-dated deglacial speleothem record of Indian Ocean climate from Socotra Island, Yemen. Earth Planet. Sci. Lett. 259, 442–456.
Smith, H.J., Fischer, H., Wahlen, M., Mastroianni, D., Deck, B., 1999. Dual modes of the carbon cycle since the Last Glacial Maximum. Nature 400, 248–250.
Takahashi, T., Sutherland, S.C., Sweeney, C., Poisson, A., Metzl, N., Tilbrook, B., Bates, N., Wanninkhof, R., Feely, R.A., Sabine, C., Olafsson, J., Nojiri, Y., 2002. Global sea–air CO_2 flux based on climatological surface ocean pCO_2, and seasonal biological and temperature effects. Deep-Sea Res. II 49, 1601–1622.
Tripati, A.K., Roberts, C.D., Eagle, R.A., 2009. Coupling of CO2 and ice sheet stability over major climate transitions of the last 20 million years. Science 326, 1394–1397.
Waelbroeck, C., Labeyrie, L., Michel, E., Duplessy, J.C., McManus, J.F., Lambeck, K., Balbon, E., Labacherie, M., 2002. Sea-level and deep water temperature changes derived from benthic foraminifera isotopic records. Quat. Sci. Rev. 21, 295–305.
Wang, Y.J., Cheng, H., Edwards, R.L., An, Z.S., Wu, J.Y., Shen, C.C., Dorale, J.A., 2001. A high-resolution absolute-dated Late Pleistocene monsoon record from Hulu cave, China. Science 294, 2345–2348.
Wang, P., Clemens, S., Beaufort, L., Braconnot, P., Gansen, G., Jian, Z., Kershaw, P., Sarnthein, M., 2005. Evolution and variability of the Asian monsoon system: state of the art and outstanding issues. Quat. Sci. Rev. 24, 595–629.
Wang, Y., Cheng, H., Edwards, R.L., Kong, X., Shao, X., Chen, S., Wu, J., Jiang, X., Wang, X., An, Z., 2008. Millenial- and orbital-scale changes in the East Asian monsoon over the past 224,000 years. Nature 224, 1090–1093.
Wanninkhof, R., 1992. Relationship between wind speed and gas exchange. J. Geophys. Res. 97, 7373–7382.
Wyrtki, K., 1973. Physical Oceanography of the Indian Ocean. Berlin, Springer-Verlag. 18–36.
Yu, J.M., 2006, Boron concentration in foraminifera as a proxy for glacial–interglacial change in the oceanic carbonate system. Ph.D. thesis, 155 pp., Univ. Cambridge, U.K.
Yu, J.M., Day, J., Greaves, M., Elderfield, H., 2005. Determination of multiple element/calcium ratios in foraminiferal calcite by quadrupole ICP-MS. Geochem. Geophys. Geosys. 6, Q08P01.
Yu, J.M., Elderfield, H., Honisch, B., 2007. B/Ca in planktonic foraminifera as a proxy for surface water pH. Paleoceanogr. 22, doi:10.1029/2006PA001347.
Yuan, D., Cheng, H., Edwards, R.L., Dykoski, C.A., Kelly, M.J., Zhang, M., Qing, J., Lin, Y., Wang, Y., Wu, J., Dorale, J.A., An, Z., Cai, Y., 2004. Timing, duration, and last transition of the last interglacial Asian monsoon. Science 304, 575–578.
Zeebe, R., Wolf-Gladrow, D., 2001. CO_2 in Seawater: Equilibrium, Kinetics, Isotopes. Elsevier, Amsterdam.